



## Article

# Kinetics of MgO Reduction in CaO-Al<sub>2</sub>O<sub>3</sub>-MgO Slag by Al in Liquid Fe

Chengsong Liu <sup>1,2</sup> , Xiaogin Liu <sup>3,\*</sup>, Xiaoliu Yang <sup>1</sup>, Hua Zhang <sup>1,\*</sup>  and Ming Zhong <sup>2</sup><sup>1</sup> The State Key Laboratory of Refractories and Metallurgy, Wuhan University of Science and Technology, Wuhan 430081, China<sup>2</sup> Department of Materials Science and Engineering, Carnegie Mellon University, Pittsburgh, PA 15213, USA<sup>3</sup> Engineering Training Center, Wuhan University of Science and Technology, Wuhan 430081, China

\* Correspondence: liuxiaoqin@wust.edu.cn (X.L.); huazhang@wust.edu.cn (H.Z.); Tel.: +86-1862-775-5628 (X.L.); +86-1321-279-9929 (H.Z.)

Received: 20 August 2019; Accepted: 6 September 2019; Published: 10 September 2019

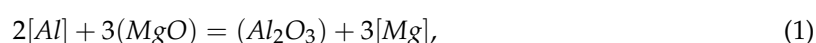


**Abstract:** Kinetics analysis without fully taking into account the effect of mass transport in slag phase on MgO reduction by Al in liquid steel would lead to overestimation of Mg pickup by steel and driving force of the reaction. Two rate models considering mass transport in (a) steel melt phase only (single control model) and (b) steel and slag melt phases (mixed control model) were developed for evaluating the thermodynamic equilibria between CaO-Al<sub>2</sub>O<sub>3</sub>-MgO slags and Al-killed steels. Calculated results from the two models were compared and then validated by equilibrium experiments between a CaO-Al<sub>2</sub>O<sub>3</sub>-MgO slag (Al<sub>2</sub>O<sub>3</sub>-saturated) and Al-killed steels with different Al levels at 1873 K (1600 °C). Results showed that the calculated reaction rate in the mixed control model was always lower than that in the single control model due to the slow mass transport in the slag phase. The mass transfer coefficient of [Mg] in the steel was computed to be  $6.2 \times 10^{-5}$  m/s from the equilibrium experiment results between an Fe-1.0 mass% Al steel and 51 mass% CaO-39 mass% Al<sub>2</sub>O<sub>3</sub>-10 mass% MgO slag at 1873 K (1600 °C), with which the mixed control model was validated at different initial Al levels in the steels.

**Keywords:** AHSS; kinetic analysis; MgO reduction reaction; mass transfer in steel and slag

## 1. Introduction

Advanced High Strength Steel (AHSS) has nowadays been widely employed in the automotive industry due to its high strength, enhanced formability and lightness. Higher levels of alloying elements such as Al, Mn, Si, and Cr have been added into the AHSS steel for better properties and energy efficiency [1–5]. In particular, the reactivity of dissolved Al in the AHSS melt proposes a significant challenge on account of undesired reactions between the molten steel and its environment including refractory liner and slags during production processes. MgO in the slag is probably reduced by the dissolved Al in the AHSS melt at a high temperature which leads to Mg transfer to the melt and unexpected changes to non-metallic inclusions, resulting in quality and performance problems of AHSS steel products. The correlative reaction and standard Gibbs free energy of MgO reduction by Al in liquid Fe are shown in Reaction (1) and Equation (2) [6], respectively, where “( )” represents that the component is presented in the mixture of oxide melt, and “[ ]” represents the dissolved element in liquid Fe. It is noteworthy that, although both MgO-containing slag and refractory can be the source of Mg in Reaction 1 [7–9], a solid spinel layer at the steel-refractory interface probably generates and prevents direct Mg pickup by the steel which turns the MgO-containing refractory to be an inefficient source of [Mg] [10–12]. This work only focused on the MgO reduction in the slag by Al in liquid Fe:



$$\Delta G_R^0 = 960746 - 321.3T \text{ (J/mol)}. \quad (2)$$

Thermodynamic and kinetic analysis on equilibrium and reactions between slags and Al-killed steels at high temperatures have been studied deeply in previous studies. Robertson et al. [13] established a mixed mass transfer control model based on diffusion-controlled reactions in slag and metal, assuming equilibrium at the slag–metal interface. Comparison of the model and experimental data including slag and steel compositions were verified at ArcelorMittal Dofasco (Hamilton, ON, Canada). Rhamdhani et al. [14] proposed an approach for accommodating the interfacial area changes in reactions between Fe–Al alloy and CaO–SiO<sub>2</sub>–Al<sub>2</sub>O<sub>3</sub> slag by employing the time-averaged interfacial area. They found that the kinetics follow a first order rate law with respect to aluminum in the metal, and were controlled by mass transport in the metal phase with a mass transfer coefficient  $k_m$  of  $1.7 \times 10^{-6}$  m/s. It also found that, although no Mg has been especially added into the molten Al-killed steels, spinel (MgO·Al<sub>2</sub>O<sub>3</sub>) inclusions still could form during refining processes as a result of MgO reduction in MgO-containing slag by Al in liquid Fe [15–17]. Harada et al. [15] established a coupled reaction model to estimate the reactions between molten steel/slag and molten steel/inclusion originating from the slag, and found the deoxidation product turned from alumina to MgO·Al<sub>2</sub>O<sub>3</sub> spinel inclusion due to an increase in the Mg content of the steel. Itoh et al. [16] studied the thermodynamics on the formation of spinel inclusions in liquid steel and evaluated the equilibrium constants and interaction parameters on calcium, magnesium, and aluminum deoxidation in liquid Fe at steelmaking temperatures by experiments. Liquid oxide phase area in the stability phase diagram of the MgO–Al<sub>2</sub>O<sub>3</sub>–CaO ternary system was determined. Park et al. [17] thought the basic way to avoid spinel inclusions was to control Mg and Al contents in molten steel other than this region. Some researchers [7,11] concluded that mass transfer of Mg in liquid steel posed a dominant effect on MgO reduction and spinel formation processes. Indeed, when there are enough MgO and Al contents reacting at the interface of Al-killed steel and MgO-containing slag, it is rather unlikely that the slag–steel reaction at such a high temperature is the rate determining step. Liu et al. [7] considered Mg transfer in molten steel was the rate controlling step of spinel generation by theoretical analysis. Okuyama et al. [11] employed the two film theory to analyze the rate-determining step of slag/metal reaction and found the rate-determining step of MgO reduction in the slag was the mass transfer of Mg through the film in molten steel. However, in the previous studies, they did not fully consider the effect of mass transport in slag phase on MgO reduction reaction, which probably would lead to overestimation of the Mg pickup by the steel and the driving force of the reaction.

In this work, reaction rate models considering mass transport in liquid Al-killed steels and CaO–Al<sub>2</sub>O<sub>3</sub>–MgO slag phases were developed. Mass transport in (a) steel melt phase only (single control model) and (b) steel and slag melt phases (mixed control model) were considered and compared in two rate models. In the first model, it was assumed that there was no boundary layer in the CaO–Al<sub>2</sub>O<sub>3</sub>–MgO slag at the steel–slag interface. The mass contents of components in the bulk slag were the same as those at the steel–slag interface, which indicated that the rate of MgO reduction reaction was just controlled by the mass transfer in the steel melt phase. In the mixed control model, the mass transport processes in both liquid Al-killed steel and CaO–Al<sub>2</sub>O<sub>3</sub>–MgO slag phase were taken into account. The interface concentrations of components in the steel and slag phases were considered to be time-dependent variables, which were determined by local equilibrium at the reaction interface. The model predictions were compared, discussed and then validated by thermodynamic equilibrium experiments between the liquid Al-killed steels and a CaO–Al<sub>2</sub>O<sub>3</sub>–MgO slag. Change in mass contents of components in the steel and slag phases were measured with time and compared with the model results.

## 2. Model Description

Generally, the chemical reactivity of Mg with oxygen is relatively higher than that of Al in molten steel according to the Ellingham diagram [18,19]. Thus, at a traditional steelmaking temperature, the standard Gibbs free energy of Reaction 1 is actually a positive value. However, MgO reduction in

MgO-containing slags and Mg pickup by liquid Al-killed steels do occur during steelmaking processes, which indicates that the reaction is not just determined by the standard Gibbs free energy but also is affected by the activities of components in the liquid Al-killed steel and MgO-containing slag phases, as well as the reaction temperature. Changes in the compositions of the liquid steel and slag depend on the fluxes of components to the reaction interface where the flux of component  $i$  across the unit area,  $J_i$ , can be defined as in Equation (3).  $m_i$  represents the mass transfer coefficient of component  $i$ , and  $C_b^i$  and  $C_i^i$  are the concentrations of component  $i$  in the bulk steel or slag and at the interface, respectively. For calculating flux rate of one species, change in composition with time is expressed as in Equation (4), where  $A$ ,  $W$  and  $\rho$  represent the reacting interface area, the weight and density of medium, respectively.  $[\text{pct } i]_b$  and  $[\text{pct } i]_i$  are converted from  $C_b^i$  and  $C_i^i$  in solvent, respectively:

$$J_i = m_i(C_b^i - C_i^i)(g \cdot m^{-2} \cdot s^{-1}), \quad (3)$$

$$\frac{d[\text{pct } i]}{dt} = -\frac{A\rho m_i}{W}([\text{pct } i]_b - [\text{pct } i]_i). \quad (4)$$

When the reaction rate models considering mass transport in liquid Al-killed steels and CaO-Al<sub>2</sub>O<sub>3</sub>-MgO slag phases were developed, composition changes of reactant and product from Reaction [1] can be obtained by solving flux equations from Equations (3) and (4) with the following assumptions:

- (a) Local equilibrium at the steel–slag interface was assumed to be achieved after a certain holding time at a high temperature;
- (b) There was no accumulation of reactants and products during reactions.

### 2.1. Single Control Model

As the rate of MgO reduction reaction is controlled by the mass transfer of liquid Al-killed steel, a schematic for changes in concentrations of [Al], [Mg] in liquid Al-killed steel and (Al<sub>2</sub>O<sub>3</sub>), (MgO) in CaO-Al<sub>2</sub>O<sub>3</sub>-MgO slag with time is shown in Figure 1. There is a compositional gradient across the reaction boundary layer on the liquid steel side, while the mass contents of slag components close to the reaction interface were the same with those in the bulk slag phase. It means that the bulk concentrations of (Al<sub>2</sub>O<sub>3</sub>) and (MgO), [%Al<sub>2</sub>O<sub>3</sub>]<sub>b</sub> and [%MgO]<sub>b</sub> should be equal to the interface concentrations of (Al<sub>2</sub>O<sub>3</sub>) and (MgO), [%Al<sub>2</sub>O<sub>3</sub>]<sub>i</sub> and [%MgO]<sub>i</sub>, respectively. In this case, there should be six unknowns: [%Al]<sub>b</sub>, [%Mg]<sub>b</sub>, [%Al<sub>2</sub>O<sub>3</sub>]<sub>b</sub> = [%Al<sub>2</sub>O<sub>3</sub>]<sub>i</sub>, [%MgO]<sub>b</sub> = [%MgO]<sub>i</sub>, [%Al]<sub>i</sub>, [%Mg]<sub>i</sub>. Rate equations for [Al], [Mg] in the liquid Al-killed steel and (Al<sub>2</sub>O<sub>3</sub>), (MgO) in the CaO-Al<sub>2</sub>O<sub>3</sub>-MgO slag phase can be expressed by Equations (5)–(8) in the single control model:

$$\frac{d[\%Al]}{dt} = -\frac{A\rho_m m_{Al}}{W_m}([\%Al]_b - [\%Al]_i), \quad (5)$$

$$\frac{d[\%Mg]}{dt} = -\frac{A\rho_m m_{Mg}}{W_m}([\%Mg]_b - [\%Mg]_i), \quad (6)$$

$$\frac{d[\%MgO]}{dt} = -\frac{3A\rho_m m_{Al} M_{MgO}}{2W_s M_{Al}}([\%Al]_b - [\%Al]_i), \quad (7)$$

$$\frac{d[\%Al_2O_3]}{dt} = \frac{1A\rho_m m_{Al} M_{Al_2O_3}}{2W_s M_{Al}}([\%Al]_b - [\%Al]_i). \quad (8)$$

A mass–balance equation between [Al] and [Mg] in the steel and a local thermodynamic equilibrium equation are shown in Equations (9) and (10)), respectively:

$$([\%Al]_b - [\%Al]_i) + \frac{2M_{Al}}{3M_{Mg}}([\%Mg]_b - [\%Mg]_i) = 0, \quad (9)$$

$$K \times h_{Al}^2 a_{MgO}^3 - h_{Mg}^3 a_{Al_2O_3} = 0. \quad (10)$$

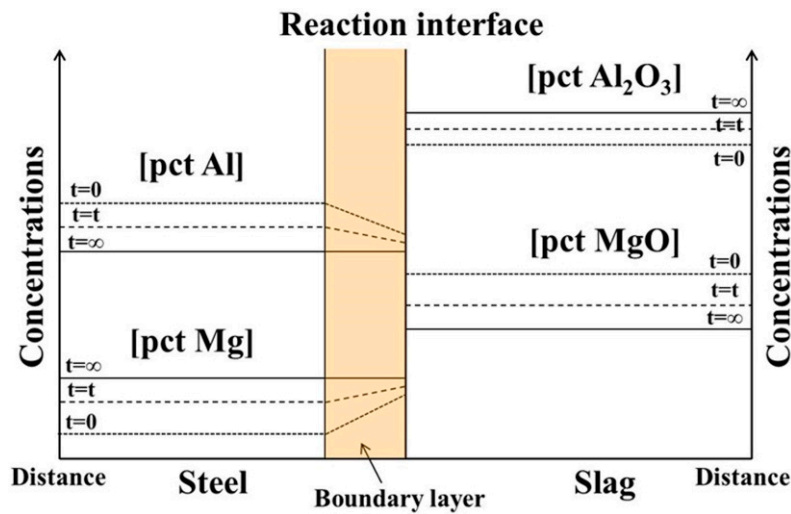


**Figure 1.** Schematic for changes in concentrations of [Al], [Mg] in liquid Al-killed steel and (Al<sub>2</sub>O<sub>3</sub>), (MgO) in CaO-Al<sub>2</sub>O<sub>3</sub>-MgO slag with time in the single control model.

## 2.2. Mixed Control Model

As the mass transport processes in both liquid Al-killed steel and CaO-Al<sub>2</sub>O<sub>3</sub>-MgO slag phases are taken into consideration, changes in mass contents of components in the reaction boundary layer on the slag side should also be considered. When Reaction (1) occurs between the steel and slag, the concentrations of (Al<sub>2</sub>O<sub>3</sub>) and (MgO) in the bulk slag, [%Al<sub>2</sub>O<sub>3</sub>]<sub>b</sub> and [%MgO]<sub>b</sub>, should gradually increase and decrease with time, respectively. Concentration gradients of (Al<sub>2</sub>O<sub>3</sub>) and (MgO) exist close to the reaction interface. Thus, there were eight unknowns: [%Al]<sub>b</sub>, [%Mg]<sub>b</sub>, [%Al<sub>2</sub>O<sub>3</sub>]<sub>b</sub>, [%MgO]<sub>b</sub>, [%Al]<sub>i</sub>, [%Mg]<sub>i</sub>, [%Al<sub>2</sub>O<sub>3</sub>]<sub>i</sub>, and [%MgO]<sub>i</sub>. Figure 2 shows a schematic for changes in concentrations of [Al], [Mg] in liquid Al-killed steel and (Al<sub>2</sub>O<sub>3</sub>), (MgO) in CaO-Al<sub>2</sub>O<sub>3</sub>-MgO slag with time in the mixed control model. Rate equations for [Al], [Mg] in the liquid Al-killed steel and (Al<sub>2</sub>O<sub>3</sub>), (MgO) in the CaO-Al<sub>2</sub>O<sub>3</sub>-MgO slag phase can be expressed by Equations (11)–(14) in the mixed control model:

$$\frac{d[\%Al]}{dt} = -\frac{A\rho_m m_{Al}}{W_m} ([\%Al]_b - [\%Al]_i), \quad (11)$$

$$\frac{d[\%Mg]}{dt} = -\frac{A\rho_m m_{Mg}}{W_m} ([\%Mg]_b - [\%Mg]_i), \quad (12)$$

$$\frac{d[\%MgO]}{dt} = -\frac{A\rho_s m_{MgO}}{W_s} ([\%MgO]_b - [\%MgO]_i), \quad (13)$$

$$\frac{d[\%Al_2O_3]}{dt} = \frac{A\rho_s m_{Al_2O_3}}{W_s} ([\%Al_2O_3]_b - [\%Al_2O_3]_i). \quad (14)$$

Three mass-balance equations among the eight unknowns and a local thermodynamic equilibrium equation are shown in Equations (15)–(17) and (10):

$$([\%Al]_b - [\%Al]_i) + \frac{2M_{Al}}{3M_{Mg}} ([\%Mg]_b - [\%Mg]_i) = 0, \quad (15)$$

$$([\%Al]_b - [\%Al]_i) - \frac{2\rho_s m_{MgO} W_m M_{Al}}{3\rho_m m_{Al} W_s M_{MgO}} ([\%MgO]_b - [\%MgO]_i) = 0, \quad (16)$$

$$([\%Al]_b - [\%Al]_i) - \frac{2\rho_s m_{Al_2O_3} W_m M_{Al}}{1\rho_m m_{Al} W_s M_{Al_2O_3}} ([\%Al_2O_3]_b - [\%Al_2O_3]_i) = 0, \quad (17)$$

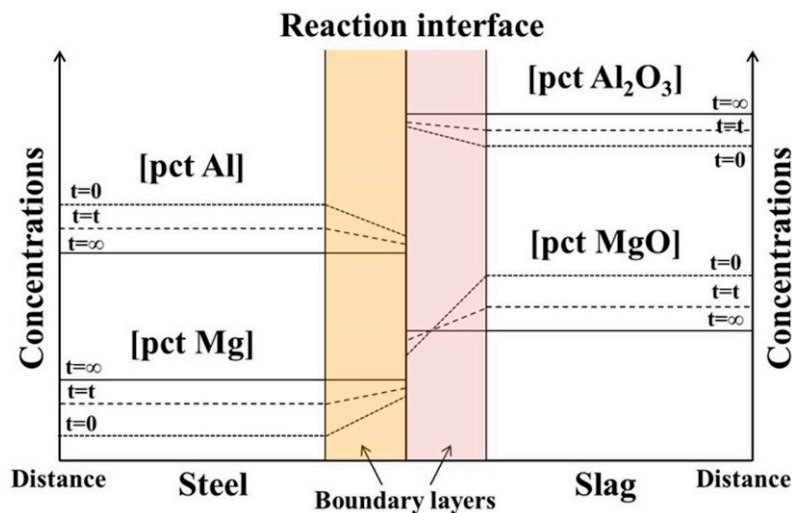


**Figure 2.** Schematic for changes in concentrations of [Al], [Mg] in liquid Al-killed steel and ( $Al_2O_3$ ), (MgO) in CaO- $Al_2O_3$ -MgO slag with time in the mixed control model

In the single control and mixed control models, activities of MgO and  $Al_2O_3$  in the CaO- $Al_2O_3$ -MgO slag at steelmaking temperatures were obtained from Ohta and Suito [20], according to the chemical composition of the slag used in the model calculations. Activities of solute  $i$  (such as Mg and Al) in the liquid Al-killed steel with respect to the 1 mass% standard state exhibiting unit activity is given by Equation (18), where  $h_i$ ,  $f_i$ , and  $[\%i]$  represent the 1 mass% activity, 1 mass% activity coefficient, and the concentration of element  $i$  in mass%, respectively. The Henrian mass% activity coefficient of solute 2 is expressed by Equation (19) as a first approximation [6], where  $e_i^j$  is the interaction parameter of  $j$  on  $i$ . These parameters will be given in Section 4:

$$h_i = f_i [\%i], \quad (18)$$

$$\log f_2 = e_2^2 [\%2] + e_2^3 [\%3] + e_2^4 [\%4] + \dots + e_2^n [\%n]. \quad (19)$$

Four differential equations and two algebraic equations for the single control model, and four differential equations and four algebraic equations for the mixed control model shown as Equations (5)–(17) were numerically solved by Matlab 2016 (MathWorks, Natick, MA, USA). Units of all parameters used in those equations can be found in Tables 1 and 2 below.

**Table 1.** Chemical compositions of the Al-killed steels and CaO- $Al_2O_3$ -MgO slag used in the equilibrium experiments.

No.	Chemical Compositions of the Steels/Mass%				Slag Composition/Mass%		
	C	Al	S/ppm	Mg/ppm	CaO	$Al_2O_3$	MgO
1	5	0.1	10	3			
2	5	1	10	3	51	39	10
3	5	2	10	3			

**Table 2.** The initial variables and their values used in the rate models.

Model Parameter	Value	Model Parameter	Value
$[\%Al]_b$ ( $t = 0$ )	0.5 mass%	Mass transfer coefficient of Al in steel, $m_{Al}$	$1 \times 10^{-4} \text{ m}\cdot\text{s}^{-1}$ [21]
$[\%Mg]_b$ ( $t = 0$ )	$3 \times 10^{-4}$ mass%	Mass transfer coefficient of Mg in steel, $m_{Mg}$	$1 \times 10^{-4} \text{ m}\cdot\text{s}^{-1}$ [21]
$[\%Al_2O_3]_b$ ( $t = 0$ )	39.0 mass%	Mass transfer coefficient of $Al_2O_3$ in slag, $m_{Al_2O_3}$	$1 \times 10^{-5} \text{ m}\cdot\text{s}^{-1}$ [13,22]
$[\%MgO]_b$ ( $t = 0$ )	10.0 mass%	Mass transfer coefficient of MgO in slag, $m_{MgO}$	$1 \times 10^{-5} \text{ m}\cdot\text{s}^{-1}$ [13,22]
$[\%CaO]_b$ ( $t = 0$ )	Balanced	Experiment temperature, $T$	1873 K (1600 °C)
$e_{Al}^{Mg}$	−0.13 [6]	Reaction area between the steel and slag, $A$	$\pi \cdot (0.03)^2 \text{ m}^2$
$e_{Al}^{Al}$	0.043 [6]	Density of steel, $\rho_{steel}$	$7000 \text{ kg}\cdot\text{m}^{-3}$
$e_{Mg}^{Al}$	0.27 [6]	Density of slag, $\rho_{slag}$	$3000 \text{ kg}\cdot\text{m}^{-3}$
$e_{Mg}^{Mg}$	0 [6]	Weight of steel, $W_{steel}$	500 g
$K$ (1873 K)	$9.74 \times 10^{-11}$ [6]	Weight of slag, $W_{slag}$	75 g

### 3. Experimental Method

Laboratorial experiments on the thermodynamic equilibrium between liquid Al-killed steels containing different Al concentrations and a CaO- $Al_2O_3$ -MgO slag ( $Al_2O_3$ -saturated) were conducted to verify the validity of the rate models. A schematic of the experimental apparatus employed in this study was shown in Figure 3. A pure electrolytic Fe and Fe-2 mass% Al steel pieces were mixed and melted in an arc melting furnace (Jinzhou Electric Co., Ltd, Jinzhou, China) at 1873 K (1600 °C) for 30 min to obtain Al-killed steel samples with different Al levels. The CaO- $Al_2O_3$ -MgO slag was prepared by mixing chemically pure CaO,  $Al_2O_3$  and MgO powders (Shanghai Macklin Biochemical Co., Ltd, Shanghai, China) in a pipe furnace (Jinzhou Electric Co., Ltd, Jinzhou, China) at 1873 K (1600 °C) for 60 min. Chemical compositions of the steel and slag samples for the equilibrium experiments were listed in Table 1. Al content in the steel ranged from 0.1 to 2.0 mass% and one 51 mass% CaO-39 mass%  $Al_2O_3$ -10 mass% MgO slag was selected. Total oxygen content in those steels averaged 20 ppm (average of several experiments over time). The quantities of the steel and slag were 500 and 75 g, respectively. Liquid steel and slag were contained in an  $Al_2O_3$  crucible (ID: 60 mm, H: 150 mm) placed in a 10 kW Ameritherm induction furnace (Jinzhou Electric Co., Ltd, Jinzhou, China) under Ar atmosphere. A Platinum–Rhodium thermocouple (Beijing Hengjiu Experiment Instrument Co., Ltd, Beijing, China) was introduced and placed above the melts to adjust the experimental temperature. After the charged steel and slag were fully melted and homogenized for 15 min, quartz tubes were then employed to take liquid steel and slag samples through an alumina guide tube during the equilibrium experiments. The moment after homogenization was set to be the start of the steel–slag reaction. Liquid steel and slag samples were taken every 5 min, quenched rapidly in water, and then analyzed by inductively coupled plasma atomic emission spectroscopy (ICP-AES) (Thermo Fisher Scientific, Waltham, MA, USA). Changes in the chemical compositions of the steels and slag in the experiments and models were compared for model validation. It should be noted that a part of inclusions such as  $Al_2O_3$  inclusions would also dissolve into the acids during ICP-AES analysis. However, according to the measurements of scanning electron microscopy and energy dispersive X-Ray spectroscopy (SEM-EDS) (JEOL, Tokyo, Japan), little inclusions were found in the steels due to extremely low oxygen concentrations (~7 ppm). Thus, the measured total Ca, Al, Mg contents have been assumed to be the dissolved ones in the steels.



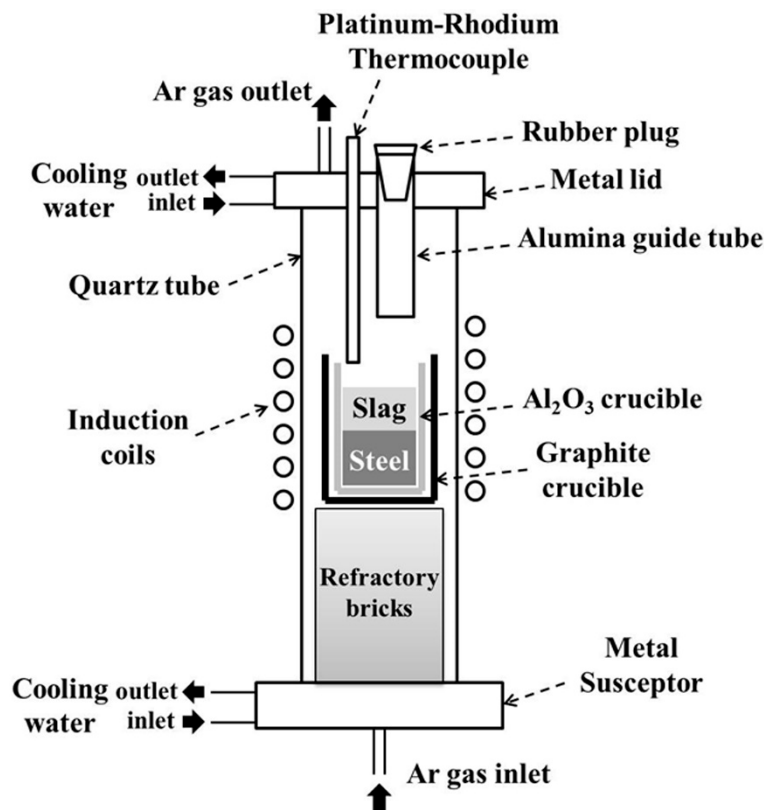


**Figure 3.** Schematic of the apparatus used for equilibrium experiments between the Al-killed steels and CaO-Al<sub>2</sub>O<sub>3</sub>-MgO slag.

## 4. Results and Discussion

### 4.1. Model Predictions and Effect of Correlative Condition

Calculations of the developed models were conducted based on these experimental conditions to check the mass balances and chemical compositions in the steels and slags from thermodynamics and kinetics. Initial variables in the models and their values are listed in Table 2. Mass transfer coefficients of Al and Mg in the steel were assumed to be the same and obtained from Harada et al. [21]. A general relationship between mass transfer coefficients and diffusivities is shown in Equation (20) in the inductively stirred melt [23]. Mass transfer coefficients of the slag components can be estimated from this equation:

$$\frac{m_1}{m_2} \cong \sqrt{\frac{D_1}{D_2}}. \quad (20)$$

Since generally the diffusion coefficient of each component in slag phase is 10–100 times smaller than that in steel phase [13,23–25], the average mass transfer coefficients of Al<sub>2</sub>O<sub>3</sub> and MgO in the slag were set as one-tenth of that in the steel. Area of reaction between the steel and slag in each equilibrium experiment was assumed to be the cross-section area of the Al<sub>2</sub>O<sub>3</sub> crucible. The effects of correlative conditions including initial [Al] and [Mg] contents in the bulk steel and (MgO) content in the bulk slag were investigated by varying their values in the model calculations. The driving force of MgO reduction by Al in the steel was also calculated and analyzed according to the bulk and interface compositions of the steel and slag in the two models.

Figure 4 shows the changes in the chemical compositions of the Al-killed steel and CaO-Al<sub>2</sub>O<sub>3</sub>-MgO slag with time in the two models using initial variables. The solid lines and dash lines denote the calculated results by the mixed control model and the single control model, respectively. The [Al] content in the steel and (MgO) content in the slag, like the reactants in Reaction 1, showed decreasing

trends, while the [Mg] content in the steel and ( $\text{Al}_2\text{O}_3$ ) content in the slag increased as reaction products in both of the kinetic models. Compared with that in the single control model, the rate of reaction was slower in the mixed control model due to the slower mass transportation in the slag. However, in both rate models, the steel and slag reached the same equilibrium compositions although through different time. Actually, there were only slight changes in the (MgO) and ( $\text{Al}_2\text{O}_3$ ) contents in the slag during the MgO reduction reaction at a high temperature, as shown in Figure 4c,d. Thus, in the model calculations, the MgO and  $\text{Al}_2\text{O}_3$  activities were assumed to be constants, which meant that they would not change with time to some extent. Calculated results by the two rate models with initial variables indicated that there was an apparent effect of mass transport in the slag phase on the reaction kinetics.

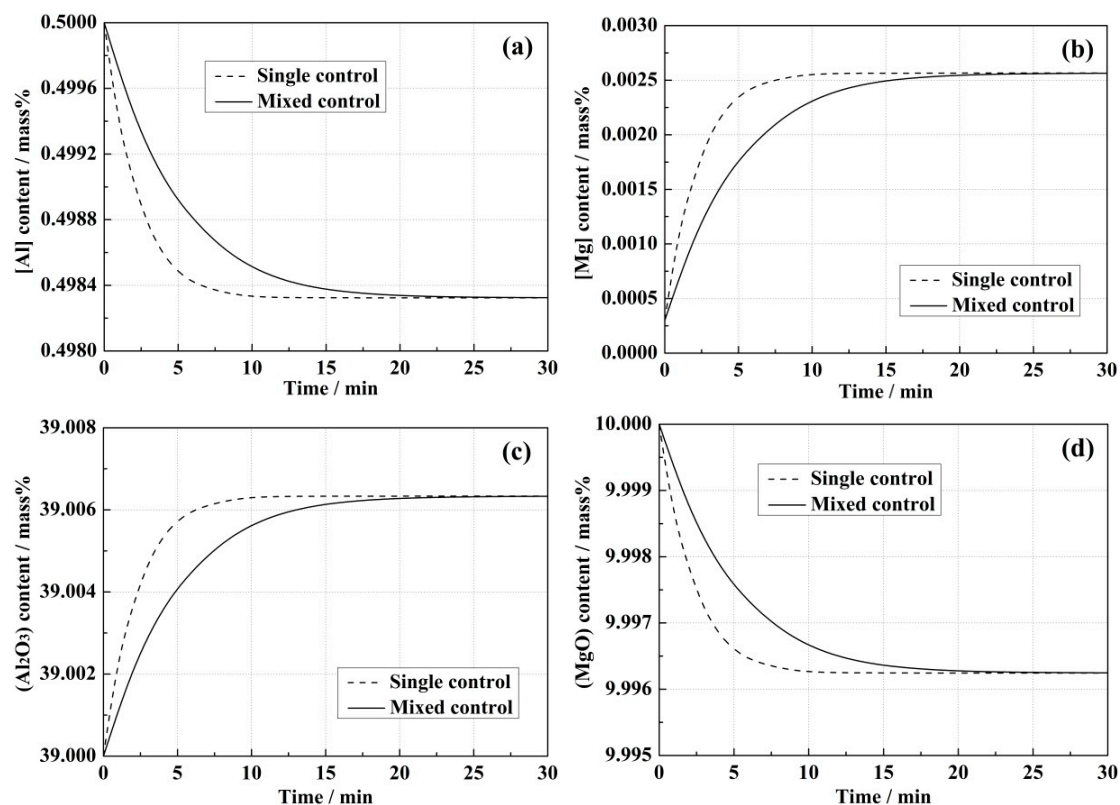


**Figure 4.** Changes in chemical compositions of the Al-killed steel and CaO- $\text{Al}_2\text{O}_3$ -MgO slag with time in the models based on initial variables: (a) [Al] content in the bulk steel; (b) [Mg] content in the bulk steel; (c) ( $\text{Al}_2\text{O}_3$ ) content in the bulk slag; and (d) (MgO) content in the bulk slag.

Figure 5 shows the effect of initial [Al] content in the Al-killed steel on the equilibrium between the steel and slag calculated by the two rate models. Since during Mg pickup reaction the consumption of [Al] was also very slight compared with the initial [Al] content in the steel, the decrease of [Al] with time was difficult to be discerned, as shown in Figure 5a. When the initial [Al] content increased from 0.5 to 2.5 mass%, the equilibrium concentrations of [Mg] in the steel and ( $\text{Al}_2\text{O}_3$ ) in the slag were also increased as the equilibrium of Reaction (1) shifted to the product side. Increase of the initial [Al] content also significantly improved the rate of the MgO reduction reaction in both kinetic models which can be observed in Figure 5b,d. Similarly, the reaction rate in the mixed control model was always lower than that in the single control model. In addition, the extent of this discrepancy between the two rate models became larger at higher [Al] levels in the Al-killed steel.



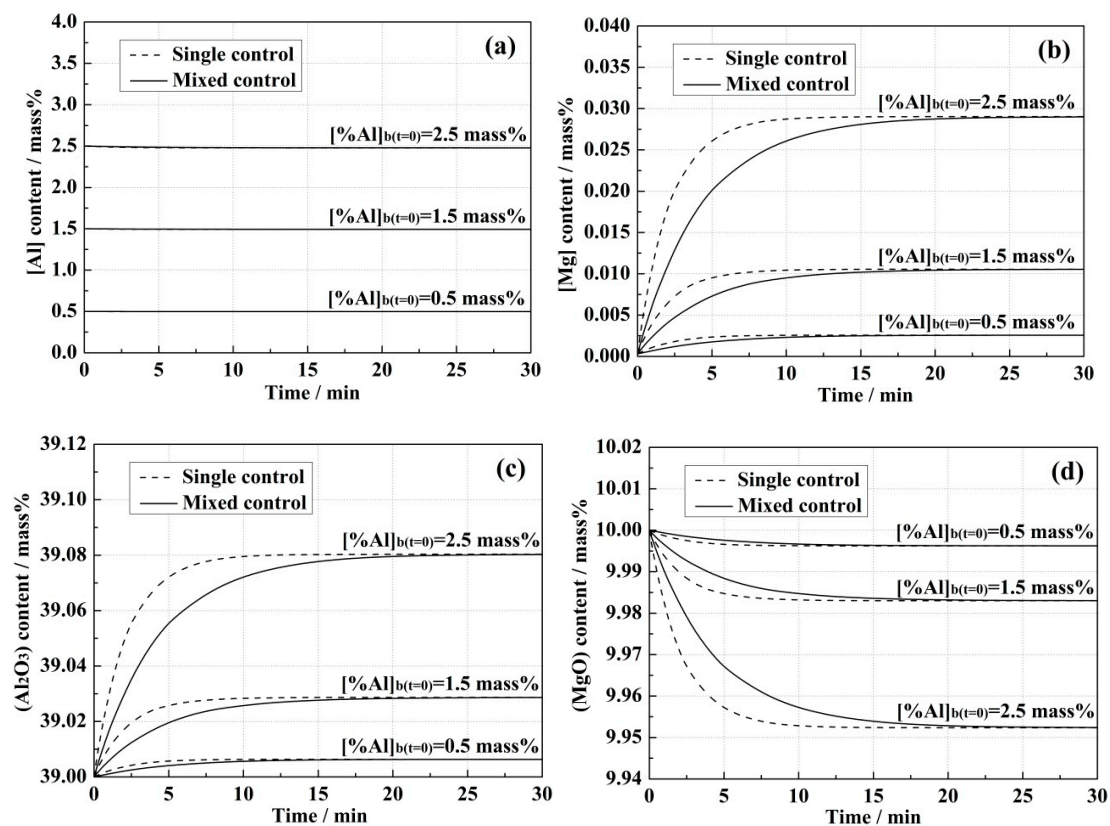


**Figure 5.** Effect of initial [Al] content in the Al-killed steel: (a) [Al] content in the bulk steel; (b) [Mg] content in the bulk steel; (c) (Al<sub>2</sub>O<sub>3</sub>) content in the bulk slag; and (d) (MgO) content in the bulk slag.

Figure 6 shows the effect of initial [Mg] content in the Al-killed steel on the equilibrium between the steel and slag calculated by the two rate models. When the initial [Mg] content in the steel,  $[\text{Mg}]_{b(t=0)}$ , varied from 3 to 10 ppm, the equilibrium concentrations of [Al] in the steel and (MgO) in the slag were increased due to the equilibrium of Reaction (1) shifting to the reactant side. The reaction rate also became lower for both models. As the initial [Mg] concentration in the steel was increased to 50 ppm, [Al] in the steel and (MgO) in the slag turned to reaction products instead of reactants which indicated that Reaction 1 has been reversed. [Mg] content in the bulk steel decreased from 50 to ~25 ppm and [Al] content increased from 0.5 to ~0.502 mass%. No matter whether it is in Reaction 1 or its reverse reaction, the reaction rates in the mixed control model were still slower than those in the single control model.

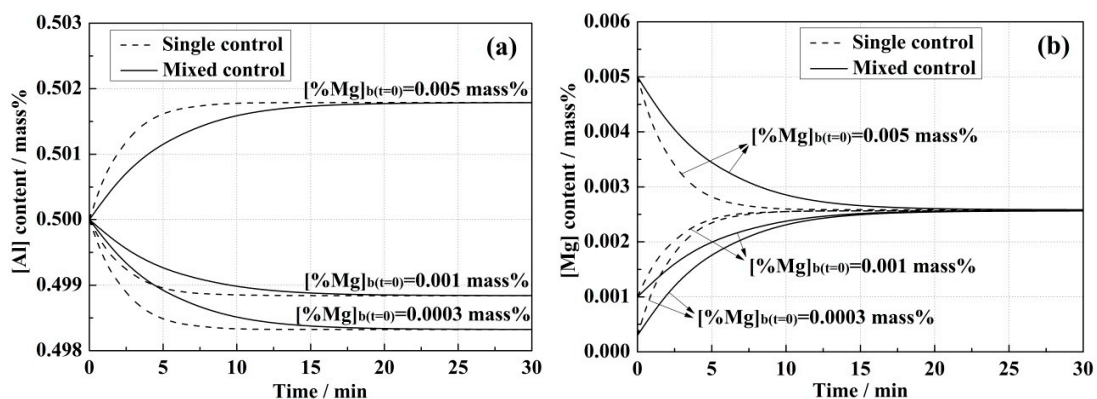


**Figure 6.** Cont.

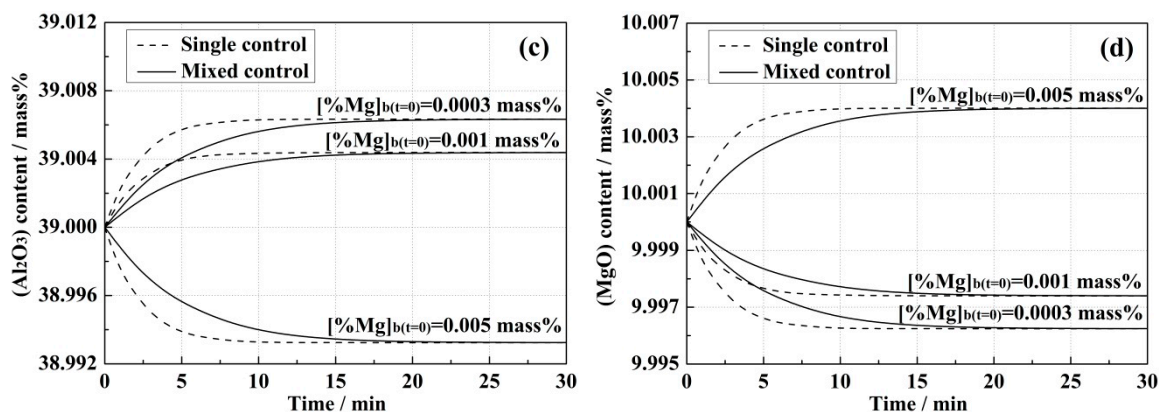


**Figure 6.** Effect of initial [Mg] content in the Al-killed steel: (a) [Al] content in the bulk steel; (b) [Mg] content in the bulk steel; (c) (Al<sub>2</sub>O<sub>3</sub>) content in the bulk slag; and (d) (MgO) content in the bulk slag.

Whether or not the CaO-Al<sub>2</sub>O<sub>3</sub>-MgO slag for refining is MgO-saturated also affects Mg pickup reaction between the steel and slag. Figure 7 shows the effect of initial (MgO) content in the CaO-Al<sub>2</sub>O<sub>3</sub>-MgO slag on the equilibrium between the steel and slag calculated by the two rate models. As the initial (MgO) content in the slag varied from 10 to 2 mass%, the equilibrium concentrations of [Mg] in the steel and (Al<sub>2</sub>O<sub>3</sub>) in the slag were decreased, as well as the rate of MgO reduction reaction. Considering that most of the refractory materials applied in the ladles' slag lines are MgO-C bricks, minimizing slag attack and MgO transfer from the refractory to molten slag should be one of the crucial aspects to suppress MgO reduction in slag and Mg pickup by liquid steel during the refining processes. In the two rate models, activities of Al<sub>2</sub>O<sub>3</sub> and MgO in the slag were dependent on the slag composition. As the initial (MgO) content decreased from 10 to 2 mass%, a general estimation on the activities of Al<sub>2</sub>O<sub>3</sub> and MgO was obtained according to the previous work by Ohta and Suito [20] for the model calculations in this study. Since mass transportation in slag was rarely considered as a rate-controlling step in kinetic models, there were no reported experimental values of mass transfer coefficients of Al<sub>2</sub>O<sub>3</sub> and MgO in liquid slag at steelmaking temperatures, which have been assumed to be an order of magnitude lower than those of solute elements in the liquid steel in the models [15,23]. Mass transfer coefficients of [Al] and [Mg] were assumed to be  $1 \times 10^{-4} \text{ m}\cdot\text{s}^{-1}$  based on previous laboratory tests [21]. This assumption has been improved and discussed on the basis of present experimental results in the latter part of this paper.

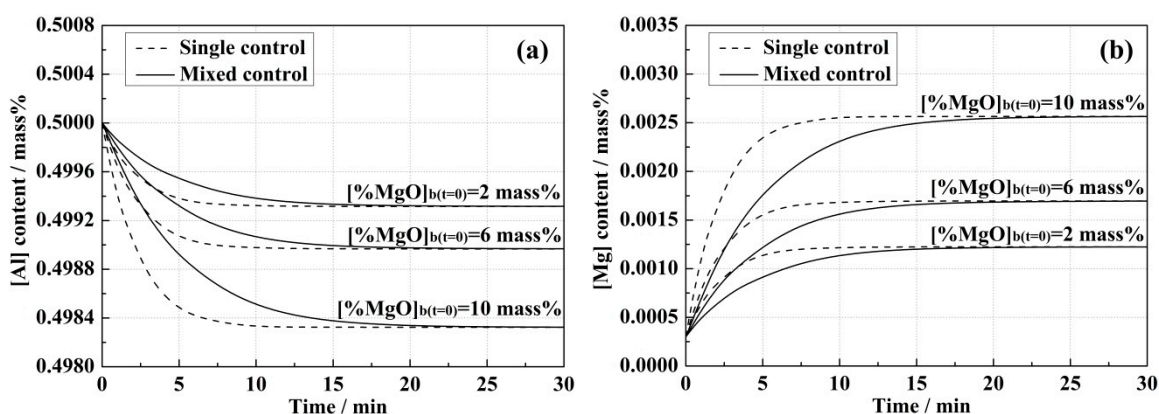


**Figure 7.** Cont.

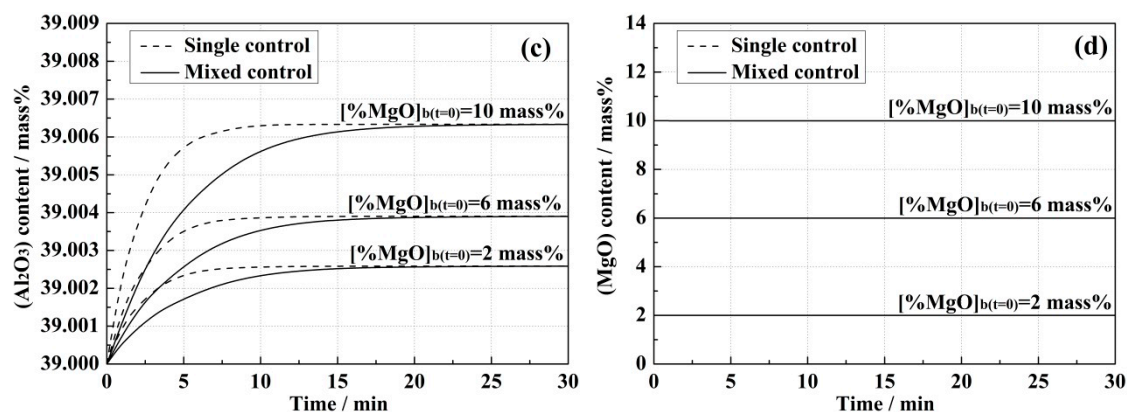


**Figure 7.** Effect of initial (MgO) content in the CaO-Al<sub>2</sub>O<sub>3</sub>-MgO slag: (a) [Al] content in the bulk steel; (b) [Mg] content in the bulk steel; (c) (Al<sub>2</sub>O<sub>3</sub>) content in the bulk slag; and (d) (MgO) content in the bulk slag.

It is thought that the difference between interface and bulk concentrations of reactants determines the driving force of the reaction. Figure 8 shows changes in bulk and interface compositions of the steel and slag in the single and mixed control models with initial variables. As shown in Figure 8a, the initial driving force in the single control model, which was considered to be the difference between the bulk and interface concentrations of [Al], was much greater than that in the mixed control model. Greater driving force leads to a higher initial reaction rate. The initial [Al] content at the interface in the mixed control model was much closer to the equilibrium value than that in the single control model. As for the [Mg] content in the steel, a similar phenomenon was confirmed. Difference between the bulk and interface concentrations of [Mg] in the single control model was larger than that in the mixed control model. Since the mass transportation in the slag was not taken into consideration in the single control model, (Al<sub>2</sub>O<sub>3</sub>) and (MgO) contents in the bulk slag were the same as those at the steel–slag interface, as shown in Figure 8c,d, respectively. However, the mass transportation of the slag components was actually slow enough to be an extra rate-limiting step. In the mixed control model, the bulk concentrations of (Al<sub>2</sub>O<sub>3</sub>) and (MgO) gradually increased and decreased with the reaction time, respectively. Concentration gradients of (Al<sub>2</sub>O<sub>3</sub>) and (MgO) existed close to the reaction interface. With the reaction time increased, the interface concentrations of (Al<sub>2</sub>O<sub>3</sub>) and (MgO) gradually became equilibrium with those in the bulk slag. The differences between the bulk and interface concentrations of (Al<sub>2</sub>O<sub>3</sub>) and (MgO) in the mixed control model are shown in Figure 8c,d, respectively, which should be taken into consideration in the kinetic calculation.

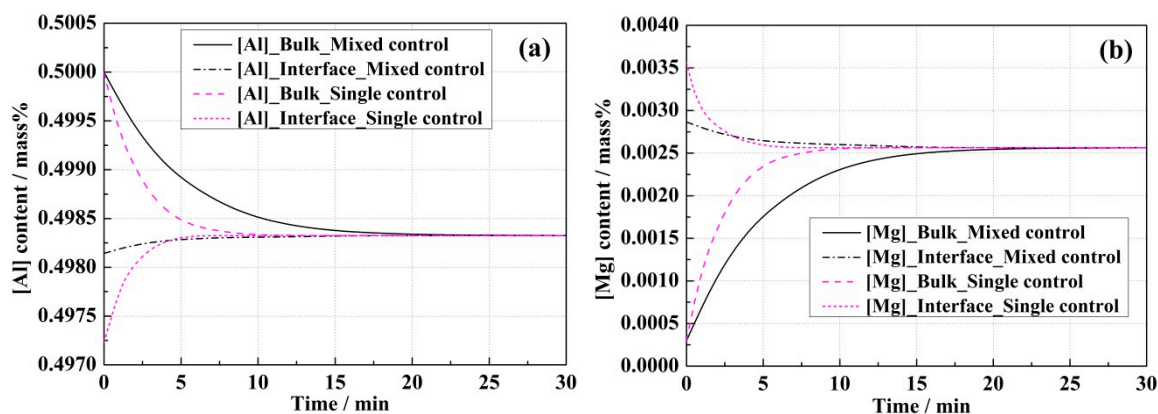


**Figure 8.** Cont.

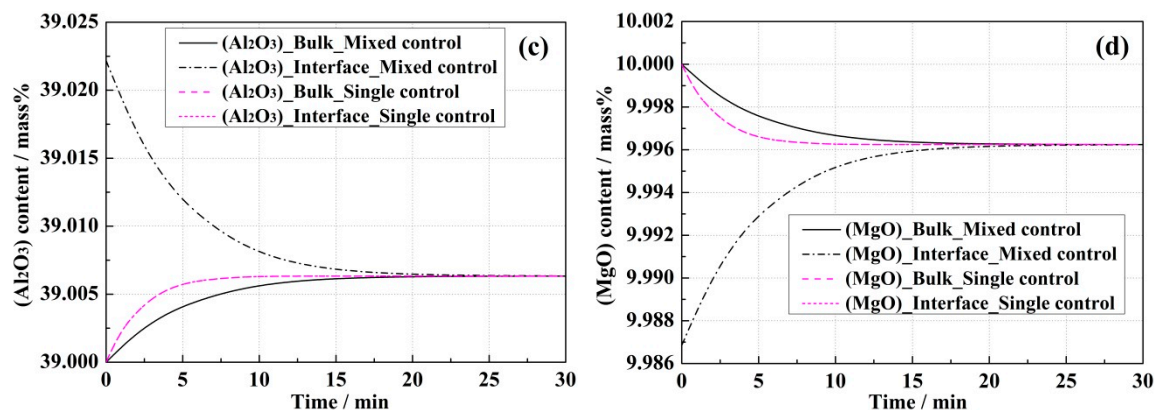


**Figure 8.** Bulk and interface compositions of the steel and slag in the single and mixed control models with initial variables: (a) [Al] content in the steel; (b) [Mg] content in the steel; (c)  $(\text{Al}_2\text{O}_3)$  content in the slag; and (d)  $(\text{MgO})$  content in the slag.

#### 4.2. Comparison Analysis of Experiment and Model Results

In Table 2, the mass transfer coefficients of Mg and Al in steel at 1873 K (1600 °C) were assumed to be  $1 \times 10^{-4} \text{ m}\cdot\text{s}^{-1}$  according to the previous work [21]. However, these mass transfer coefficients in liquid steel also can be measured and obtained based on the experimental results in this study. Experimental changes of [Mg] and [Al] contents in the steel with time in experiment 2 where  $[\% \text{Al}]_{\text{b}}(t=0)$  equaled 1.0 mass% are shown in Table 3. The mass transfer coefficient of [Mg] in steel,  $m_{\text{Mg}}$ , can be computed from this case according to Equation (21) [26], where  $[\% \text{Mg}]_{\text{b},t=0}$ ,  $[\% \text{Mg}]_{\text{b},t=t}$  and  $[\% \text{Mg}]_{\text{b},\text{eq}}$  represent [Mg] content in the bulk steel at  $t = 0$ ,  $t = t$  and at equilibrium.  $V$  represents the volume of liquid steel in present study. After the calculation,  $m_{\text{Mg}}$  was obtained to be  $6.2 \times 10^{-5} \text{ m/s}$  when a flat reaction interface was assumed. The mass transfer coefficient of [Al] was assumed to be the same as that of [Mg] in the steel. This value was also employed to the other two experiments where  $[\% \text{Al}]_{\text{b}}(t=0)$  equaled 0.5 and 2.0 mass%, respectively. Both calculation and experiment results demonstrated that the changes of  $[\text{Al}_2\text{O}_3]$  and  $[\text{MgO}]$  contents in the slag were very slight compared with their initial contents. Here, in Figure 9, changes of [Mg] and [Al] concentrations with time in the equilibrium experiments were displayed and then compared with the calculated results in the single and mixed control models using the adjusted mass transfer coefficients in the steel:

$$\lg \frac{[\% \text{Mg}]_{\text{b},t=0} - [\% \text{Mg}]_{\text{b},\text{eq}}}{[\% \text{Mg}]_{\text{b},t=t} - [\% \text{Mg}]_{\text{b},\text{eq}}} = \frac{m_{\text{Mg}}}{2.3} \cdot \frac{A}{V} \cdot t. \quad (21)$$

**Table 3.** The initial variables and their values used in the rate models.

Time/min	0	5	10	15	20	25	30
$[\% \text{Mg}]_{\text{b}}/\text{ppm}$	3	32.6	52.2	51.5	47.7	57.3	58.5
$[\% \text{Al}]_{\text{b}}/\text{mass}\%$	1.0	0.98	0.97	0.92	0.94	0.92	0.9

Figure 9 indicates the value of mass transfer coefficient in the steel, which was computed from the change in [Mg] content in experiment 2, where  $[\% \text{Al}]_{\text{b}}(t=0)$  equaled 1.0 mass%, was also suitable for lower and higher [Al] levels. Predicted [Mg] and [Al] concentrations of the liquid steel in the mixed control model during equilibrium matched the experimental results well, which demonstrated that the rate of Mg pickup reaction followed the mixed control model other than the single control model. A degree of inevitable reoxidation probably led to the deviations between the predicted and experimental values. On one hand, the single control model was actually a sub-model of the mixed control model, which was only valid in extreme cases where MgO flux from the  $\text{CaO-Al}_2\text{O}_3\text{-MgO}$  bulk slag to the reaction interface was large enough to neglect its rate limitation. However, in this



study, although the CaO-Al<sub>2</sub>O<sub>3</sub>-MgO slag was Al<sub>2</sub>O<sub>3</sub>-saturated, the effect of mass transportation in the slag on the reaction kinetics was still observed and confirmed. On the other hand, according to the present study, it was demonstrated that MgO reduction reaction would be restrained by insufficient slag flux to the interface, such as MgO flux. Thus, giving full consideration to the mass transportation in the slag has improved the accuracy of kinetics model for predicting the equilibrium between the CaO-Al<sub>2</sub>O<sub>3</sub>-MgO slag and the Al-killed steel. The interface concentrations of the steel and slag should also be treated carefully, which determine the driving force of the MgO reduction reaction.

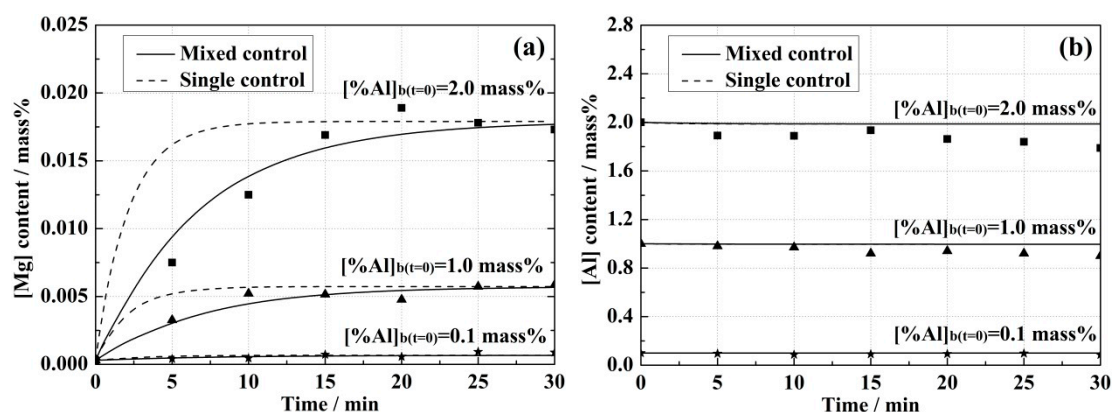


**Figure 9.** Comparison of experimental steel compositions with calculated results in the single and mixed control models using the adjusted mass transfer coefficients in the steel: (a) [Mg] content; and (b) [Al] content.

Determining how much the model output is changed by the variation in input parameters is essential to calibrate and validate the models. In this study, the sensitivity analyses of the models were studied by simply varying values of correlative parameters during calculation. However, Vu-Bac et al. [27,28] proposed a sensitivity analysis toolbox for quantifying the influence of uncertain input parameters on uncertain model outputs. They compared the sensitivity indices in the spline regression model and polynomial regression model with analytical results, and found the difference between numerical results in the spline regression model and analytical results due to the noise and the reduced COD is insignificant. This work can be a new method applied in this study for more accurately estimating the effect of industrial and experimental conditions on kinetics of MgO reduction in CaO-Al<sub>2</sub>O<sub>3</sub>-MgO Slag by Al in liquid Fe. In addition, equilibrium between the steel and inclusions has not been taken into consideration by achieving clean steel with little inclusions in the experiments. When a large number of oxide inclusions such as spinel or complex CaO-Al<sub>2</sub>O<sub>3</sub>-MgO inclusions formed in liquid steel, they would become another driving force for MgO reduction and Mg pickup reactions. More Mg content would transfer from the CaO-Al<sub>2</sub>O<sub>3</sub>-MgO bulk slag to the steel, and then to form those inclusions. Under that condition, the consumption of Mg in the steel by oxide inclusions should also be fully considered. Additional studies are needed to examine the effect of steel-inclusion reactions on kinetics of MgO reduction in the CaO-Al<sub>2</sub>O<sub>3</sub>-MgO slags by Al in liquid Fe.

## 5. Conclusions

In order to evaluate the kinetics of MgO reduction in CaO-Al<sub>2</sub>O<sub>3</sub>-MgO slags by Al in liquid steel, two rate models considering mass transportation in (a) steel melt phase only (single control model) and (b) steel and slag melt phases (mixed control model) were developed. The following conclusions were obtained:

1. Due to the slow mass transport in the slag, the reaction rate in the mixed control model was always lower than that in the single control model.

2. Higher initial [Al] content in the steel and (MgO) content in the slag led to the increase of equilibrium concentrations of [Mg] in the steel and ( $\text{Al}_2\text{O}_3$ ) in the slag, and also improved the reaction rates in both kinetic models.
3. In the single control model, ( $\text{Al}_2\text{O}_3$ ) and (MgO) contents in the bulk slag were the same as those at the steel–slag interface, while differences between the bulk and interface concentrations of ( $\text{Al}_2\text{O}_3$ ) and (MgO) were observed in the mixed control model, which resulted in the mass transportation of the slag components being an extra rate-limiting step.
4. The mass transfer coefficient of [Mg] in the steel was computed to be  $6.2 \times 10^{-5} \text{ m}\cdot\text{s}^{-1}$  according to the experimental equilibrium results between an Fe-1.0 mass% Al steel and 51 mass% CaO-39 mass%  $\text{Al}_2\text{O}_3$ -10 mass% MgO slag at 1873 K (1600 °C). Using this value, the mixed control model was validated at different initial Al levels in the steels.
5. Experimental results with the model predictions confirmed that the mass transport in the slag should be given full consideration during the kinetics analysis of MgO reduction reaction.

**Author Contributions:** Conceptualization, C.L. and H.Z.; methodology, X.L.; validation, X.Y. and M.Z.; formal analysis, X.L.; investigation, C.L., H.Z. and M.Z.; writing—original draft preparation, C.L.; writing—review and editing, X.L.; funding acquisition, C.L. and H.Z.

**Funding:** This research was funded by the National Key R & D Program of China, Grant No. 2017YFB0304201 and the National Natural Science Foundation of China, Grant Nos. 51604201 and 51774217.

**Acknowledgments:** The authors are grateful to the support by the scholarship from the China Scholarship Council (CSC) under the Grant CSC No. 201708420228.

**Conflicts of Interest:** The authors declare no conflict of interest.

## References

1. Aydin, H.; Essadiqi, E.; Jung, I.H.; Yue, S. Development of 3rd generation AHSS with medium Mn content alloying compositions. *Mater. Sci. Eng. A* **2013**, *564*, 501–508. [\[CrossRef\]](#)
2. Khan, M.I.; Kuntz, M.L.; Biro, E.; Zhou, Y. Microstructure and mechanical properties of resistance spot welded advanced high strength steels. *Mater. Trans.* **2008**, *49*, 1629–1637. [\[CrossRef\]](#)
3. Zhou, M.X.; Xu, G.; Tian, J.Y.; Hu, H.J.; Yuan, Q. Bainitic transformation and properties of low carbon carbide-free bainitic steels with Cr addition. *Metals* **2017**, *7*, 263. [\[CrossRef\]](#)
4. Zhou, W.; Wu, K.M.; Zhong, L.; Zhang, C.; Hou, T.P.; Misra, R.D.K. A comparative study on the dynamic tensile behavior of nanostructured bainitic and quenched-tempered martensitic steels. *Metals* **2018**, *8*, 728. [\[CrossRef\]](#)
5. Guo, J.; Seo, M.D.; Shi, C.B.; Cho, J.W.; Kim, S.H. Control of crystal morphology for mold flux during high-aluminum AHSS continuous casting process. *Metall. Mater. Trans. B* **2016**, *47*, 2211–2221. [\[CrossRef\]](#)
6. Hino, M.; Ito, K. *Thermodynamic Data for Steelmaking*, 1st ed.; Tohoku University Press: Sendai, Japan, 2010; pp. 10–24, 74, 82.
7. Liu, C.; Huang, F.; Suo, J.; Wang, X. Effect of magnesia-carbon refractory on the kinetics of  $\text{MgO}\cdot\text{Al}_2\text{O}_3$  spinel inclusion generation in extra-low oxygen steels. *Metall. Mater. Trans. B* **2016**, *47*, 989–998. [\[CrossRef\]](#)
8. Deng, Z.; Zhu, M.; Sichen, D. Effect of refractory on nonmetallic inclusions in Al-killed steel. *Metall. Mater. Trans. B* **2016**, *47*, 3158–3167. [\[CrossRef\]](#)
9. Mu, H.Y.; Zhang, T.S.; Fruehan, R.J.; Webler, B.A. Reduction of CaO and MgO slag components by Al in liquid Fe. *Metall. Mater. Trans. B* **2018**, *49*, 1665–1674. [\[CrossRef\]](#)
10. Verma, N.; Pistorius, P.C.; Fruehan, R.J.; Potter, M. Modification of spinel inclusions by calcium in liquid steel. *Iron Steel Technol.* **2010**, *7*, 189–197.
11. Okuyama, G.; Yamaguchi, K.; Takeuchi, S.; Sorimachi, K. Effect of slag composition on the kinetics of formation of  $\text{Al}_2\text{O}_3$ –MgO inclusions in aluminum killed ferritic stainless steel. *ISIJ Int.* **2000**, *40*, 121–128. [\[CrossRef\]](#)
12. Kumar, D.; Pistorius, P.C. Rate of MgO pickup in alumina inclusions in aluminum-killed steel. *Metall. Mater. Trans. B* **2019**, *50*, 181–191. [\[CrossRef\]](#)



13. Robertson, D.G.C.; Deo, B.; Ohguchi, S. A multicomponent mixed transport control theory for the kinetics of coupled slag/metal and slag/metal/gas reactions: Application to de sulphurization of molten iron. *Ironmak. Steelmak.* **1984**, *11*, 41–55.
14. Rhamdhani, M.A.; Brooks, G.A.; Coley, K.S. Kinetics of metal/slag reactions during spontaneous emulsification. *Metall. Mater. Trans. B* **2005**, *36*, 219–227. [[CrossRef](#)]
15. Harada, A.; Maruoka, N.; Shibata, H.; Kitamura, S.Y. A kinetic model to predict the compositions of metal, slag and inclusions during ladle refining: Part 1. Basic concept and application. *ISIJ Int.* **2013**, *53*, 2110–2117. [[CrossRef](#)]
16. Itoh, H.; Hino, M.; Ban-ya, S. Thermodynamics on the formation of spinel nonmetallic inclusion in liquid steel. *Metall. Mater. Trans. B* **1997**, *28*, 953–956. [[CrossRef](#)]
17. Park, J.H.; Todoroki, H. Control of MgO·Al<sub>2</sub>O<sub>3</sub> spinel inclusions in stainless steels. *ISIJ Int.* **2010**, *50*, 1333–1346. [[CrossRef](#)]
18. Richardson, F.D.; Jeffes, J.H.E. The thermodynamics of substances of interest in iron and steel making. III—sulphides. *J. Iron Steel Inst.* **1952**, *171*, 165–175.
19. Alcock, J.C.B.; Easterbrook, E. Aluminum and Aluminum Alloy. In *Corrosion*, 1st ed.; Butterworth-Heinemann: London, UK, 1994; pp. 3–37.
20. Ohta, H.; Suito, H. Activities in CaO-MgO-Al<sub>2</sub>O<sub>3</sub> slags and deoxidation equilibria of Al, Mg, and Ca. *ISIJ Int.* **1996**, *36*, 983–990. [[CrossRef](#)]
21. Harada, A.; Miyano, G.; Maruoka, N.; Shibata, H.; Kitamura, S. Dissolution behavior of Mg from MgO into molten steel deoxidized by Al. *ISIJ Int.* **2014**, *54*, 2230–2238. [[CrossRef](#)]
22. Kitamura, S.; Kitamura, T.; Shibata, K.; Mizukami, Y.; Mukawa, S.; Nagakawa, J. Effect of stirring energy, temperature and flux composition on hot metal dephosphorization kinetics. *ISIJ Int.* **1991**, *31*, 1322–1328. [[CrossRef](#)]
23. Park, J.W.; Sridhar, S.; Fruehan, R.J. Kinetics of reduction of SiO<sub>2</sub> in SiO<sub>2</sub>-Al<sub>2</sub>O<sub>3</sub>-CaO slags by Al in Fe-Al(-Si) melts. *Metall. Mater. Trans. B* **2014**, *45*, 1380–1388. [[CrossRef](#)]
24. Monaghan, B.J.; Nightingale, S.A.; Chen, L.; Brooks, G.A. The Dissolution Behavior of Selected Oxides in CaO-SiO<sub>2</sub>-Al<sub>2</sub>O<sub>3</sub> Liquid Oxides. In Proceedings of the VII International Conference Molten Slags, Fluxes and Salts, Cape Town, South Africa, 25–28 January 2004; The South African Institute of Mining and Metallurgy: Johannesburg, South Africa, 2004.
25. Elizaveta, C. Dissolution Kinetics of CaO and MgO in Converter Steelmaking Slags. Ph.D. Thesis, University of Leoben, Leoben, Styria, Austria, 2016.
26. Huang, X.H. *Mechanism of Ferrous Metallurgy*, 4th ed.; Metallurgical Industry Press: Beijing, China, 2013; pp. 120–122.
27. Vu-Bac, N.; Lahmer, T.; Zhuang, X.; Nguyen-Thoi, T.; Rabczuk, T. A software framework for probabilistic sensitivity analysis for computationally expensive models. *Adv. Eng. Softw.* **2016**, *100*, 19–31. [[CrossRef](#)]
28. Hamdia, M.K.; Ghasemi, H.; Zhuang, X.Y.; Alajlan, N.; Rabczuk, T. Sensitivity and uncertainty analysis for flexoelectric nanostructures. *Comput. Methods Appl. Mech. Eng.* **2018**, *337*, 95–109. [[CrossRef](#)]

